Soft Matter

ARTICLE TYPE

Cite this: DOI: 00.0000/xxxxxxxxxx

Probing wetting properties with self-propelled droplets†

Bernardo Boatini,* Cristina Gavazzoni,Leonardo Gregory Brunnet and Carolina Brito[a]

Received Date
Accepted Date

DOI: 00.0000/xxxxxxxxxx

Wetting phenomena are relevant in several technological applications, particularly those involving hydrophobic or hydrophilic surfaces. Many substrates support multiple wetting states depending on surface conditions or droplet history —a behavior known as metastability. This feature is crucial both for its theoretical complexity and for its relevance in practical applications that rely on controlling metastable states. While several experimental and computational techniques have been developed to study metastability, they tend to be complex or computationally expensive. In this work, we introduce an alternative approach based on concepts from active matter physics. We investigate the wetting behavior of a droplet placed on a pillared surface using a 3-spin Cellular Potts model with a polarity term that mimics a self-propelled droplet. Applying this model to a pillared substrate with known metastable wetting states, we demonstrate that increasing activity enables the droplet to traverse free energy barriers, explore consecutive metastable states, and eventually suppress metastability entirely. Our results show that activity reduces the disparity between dry and wet states and provides a reliable framework for identifying and quantifying metastability through contact angle measurements.

The study of wetting phenomena is of great interest due to its wide range of technological applications involving hydrophobic and hydrophilic surfaces. Significant effort has been made to understand droplet behavior on rough solids, aiming to design substrates with controlled wetting properties[1–6]. Since the foundational work of Wenzel[7] and Cassie-Baxter[8], the concept of apparent contact angle has become central, accounting for intrinsic wettability and surface heterogeneities. Some models have since emerged based on surface chemistry and topography, yet most rely on the equilibrium assumption, which means that the droplet adopts a single, stable wetting state. In reality, however, surfaces can support metastable states, where the droplet is locally trapped, leading to effects like contact angle hysteresis[9–11].

Metastability is common in wetting and poses both theoretical challenges and practical relevance. For example, superhydrophobicity often relies on metastable states[9], while super-slippery surfaces aim to eliminate them[12]. Therefore, understanding and controlling metastability is key to engineering advanced functional substrates.

Experimentally and computationally, probing metastable states is difficult, as it requires extensive trials. Some methods include observing droplets from below[13] or using varied initial conditions[14–16]. Computational tools like umbrella sampling and adaptive biasing[17] have proven useful but are often complex and resource-intensive.

To overcome local energy barriers, experiments often introduce initial droplet velocity or substrate vibrations[9]. Inspired by this, a promising route is continuous, nonequilibrium energy injection—such as self-propulsion. This can be achieved via engineered surfaces, coalescence, or external fields[18–21]. More generally, active matter systems, where internal agent dynamics drive motion, provide a compelling framework for understanding this phenomenon[22–27].

While some numerical and experimental studies have explored how active suspensions alter wetting on flat surfaces[28–30], their implications for the metastability paradigm in wetting physics remain largely unexplored.

In this work, we apply principles and methods from active matter physics to probe the wetting properties of a substrate and characterize its metastability. We simulate the system using a 3-spin Cellular Potts Model. Activity is modeled via a polarity term[31] in the energy functional, which drives a time-varying directional bias in the droplet's dynamics. This mimics a self-propelled droplet that exhibits isotropic motion, similar to what is shown in previous experimental results with self-propelled droplets[32–35]. This model is employed to investigate the wetting behavior on a pillared surface, a substrate whose wetting properties are well understood in the absence of the activity term. In particular, the pillared surface is known to have several metastable states, ranging from dry to wet, depending on its roughness[6,15,17]. Here we show that, for certain substrate roughness, increasing activity causes the droplet to transition through consecutive free energy minima and, beyond a certain threshold, can even suppress

* *Instituto de Física, Universidade Federal do Rio Grande do Sul, Caixa Postal 15051, CEP 91501-970, Porto Alegre, Rio Grande do Sul, Brazil; E-mail: b.boattini@gmail.com*

† Supplementary Information available: [details of any supplementary information available should be included here]. See DOI: 10.1039/cXsm00000x/

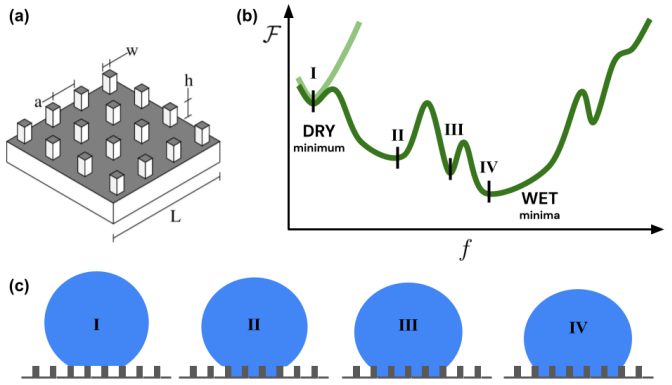

Fig. 1 **(a)** Definition of the geometric parameters of the pillared surface: roughness ratio $r = 1 + 4hw/(a+w)^2$, where a is the inter-pillar distance, w is the pillar width and h is the pillar height; L is the system size. **(b)** Schematic representation of the free energy $\mathcal{F}$ as a function of the water fraction penetrating the substrate f, based on results from two distinct pillared surfaces in Ref.[17]. The light-green curve, which exhibits a single minimum, corresponds to a surface with a high roughness ratio r, whereas the dark-green curve, displaying multiple local minima, represents substrates with lower r. **(c)** Cross-sectional representations of the water droplet at each minimum of $\mathcal{F}$, arranged from the driest to the wettest state (I–IV).

metastable behavior entirely. Overall, higher self-propulsion reduces the disparity between the driest and wettest metastable states. This allows us to clearly identify whether a substrate exhibits metastability and to estimate the number of local minima while simultaneously measuring the associated contact angles.

This work is organized as follows. Section 1 introduces the parameters of the pillared surface studied in this work and reviews its wetting properties as established in previous studies. In Section 2, we present the numerical model used, along with the initial conditions employed in the simulations to investigate metastability. Section 3 presents and discusses the main results, followed by Section 4, which contains our conclusions.

1 Metastability of a pillared surface

Metastability is often understood in terms of a complex landscape of a system's thermodynamic potential. In this framework, systems that exhibit metastability are interpreted as having local minima in their free energy landscape, separated by barriers that may depend on one or more system variables.

In the context of wetting phenomena, a metastable state corresponds to a particular wetting configuration. These configurations typically fall into two categories: dry states, where the droplet does not fully infiltrate the substrate, and wet states, where the droplet penetrates the surface texture. Dry states are commonly referred to as Cassie–Baxter (CB) states, while wet states are known as Wenzel (WE) states. Each state is characterized by its apparent contact angle θ_C and a filling fraction f, which quantifies the portion of liquid that penetrates the substrate relative to the whole droplet.

The wetting properties of a droplet placed on a pillared substrate have been explored in recent works[15,17,36]. The geometry of the pillared surface is determine by a pillar height h, a pillar width w and an inter-pillar distance a (Figure 1(a)) and the roughness ratio r of this surface is given by $r = 1 + 4hw/(a+w)^2$.

Using a 3-spin cellular Potts model (described in the next section) and a continuous model that minimizes the global interfacial energy, it was shown that the final wetting state of a droplet depends on its initial condition[15] as previously observed experimentally[9,14]. A droplet initially placed in a dry state would remain in a (another) dry state with a high contact angle, even though this state were not the most energetically favorable one according to the continuous model. On the other hand, if the droplet was initially placed wetting the substrate, the final state obtained in the simulation would correspond to the thermodynamically stable configuration.

To better investigate this behavior, it was performed a combination of constrained Monte Carlo simulations and the string method to compute the free energy profile of a liquid droplet deposited on a pillared surface as a function of the water fraction penetrating the surface f[17]. A schema of the result is illustrated in Figure 1(b). The results reveal that for a certain range of geometric parameters (specifically, those associated with high surface roughness) the substrate exhibits a single free energy minimum, corresponding to a superhydrophobic wetting state. As the surface roughness decreases, the number of local minima in the free energy profile increases, indicating the emergence of one dry metastable state and multiple wet states (Figure 1(c)).

2 Numerical Model

2.1 The Cellular Potts Model (CPM)

The Cellular Potts Model (CPM), originally introduced by Graner and Glazier[37], has been widely used to study wetting phenomena in textured surfaces[38,39], in particular, wetting of pillared surfaces[6,15,36].

We begin with the 3D CPM, defined on a simple cubic lattice. The system is governed by the following Hamiltonian:

$$\begin{aligned} H_0 &= \frac{1}{2}\sum_{<\mathrm{i,j}>} E_{s_\mathrm{i},s_\mathrm{j}}(1-\delta_{s_\mathrm{i},s_\mathrm{j}}) + \lambda\left(\sum_\mathrm{i}\delta_{s_\mathrm{i},1} - V_T\right)^2 \\ &+ mg\sum_\mathrm{i} h_\mathrm{i}\delta_{s_i,1} \end{aligned} \tag{1}$$

where the spin $s_i \in \{0,1,2\}$ represent gas, water and solid states, respectively (Figure 2(a)).

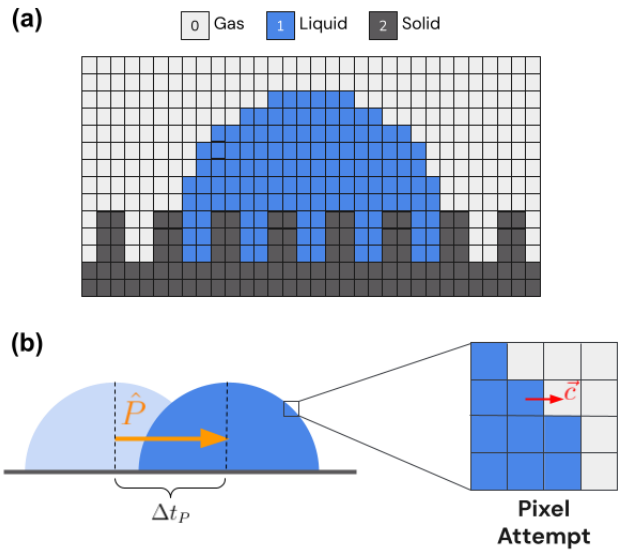

Fig. 2 (a) Schematic cross-section of a 3D droplet over a pillared substrate in the Cellular Potts Model (CPM). Each pixel corresponds to a different state ($s_i = 0, 1, 2$). (b) Representation of the activity term, Eq. 2. The displacement of the droplet's center of mass is measured at intervals of Δt_P (in Monte Carlo Steps, MCS). The vectors $\vec{P}$ (orange) and $\vec{c}$ (red) are planar and interact only within the horizontal plane.

The first term in Eq.(1) represents the energy related to the presence of interfaces between sites of different types. The summation ranges over pairs of neighbors which comprise the 3D Moore neighborhood in the simple cubic lattice (26 sites, excluding the central one), E_{s_i,s_j} is the interaction energies of sites s_i and s_j of different states at interfaces and δ_{s_i,s_j} is the Kronecker delta. The second term is responsible to keep the droplet volume around a target volume V_T. The summation is over the pixels of water and λ represents the compressibility of the water. The last term is the gravitational energy associated to the droplet.

In our simulations the length scale is such that one lattice spacing corresponds to 1 μm and the surface tensions values are divided by 26, which is the number of neighbors that contributes to the first summation of our Hamiltonian. Therefore, the interfacial interaction energies $E_{s_i,s_j} = A\sigma_{s_i s_j}$, with $A = 1\mu\text{m}^2$ are given by $E_{0,1} = 2.70 \times 10^{-9}\mu$J, $E_{0,2} = 0.96 \times 10^{-9}\mu$J and $E_{1,2} = 1.93 \times 10^{-9}\mu$J. The mass in a unit cube is $m^w = 10^{-15}$kg and $\lambda = 0.01 \times 10^{-9}\mu\text{J}/(\mu\text{m})^6$. This defines what we refer to as the *passive case droplet*, which serves as the starting point for implementing its active counterpart.

2.2 A self-propelled droplet: the CPM with activity

There are several ways to achieve self-propulsion in a droplet, ranging from the design of specialized surfaces to merging processes or even the application of external fields[18–21,40]. In this work, we focus specifically on isotropic and Brownian-like motions, where the droplet exhibits random motion without any intentional directional control driven by external forcing. This type of behavior was already reported on experimental literature, and can be characterized as a persistent Brownian motion[32–34].

In such systems, the energy is generally injected trough the constitutive agents of the droplet solution, which then characterizes it as a active matter suspension. To incorporate this feature in the model, an additional term is added to the variation of the Hamiltonian when a spin is changed: $\Delta H = \Delta H_0 + \Delta H_\alpha$, where the additional term is given by[31,41]

$$\Delta H_\alpha = -\mu \widehat{P}(t - \Delta t_P) \cdot \vec{c} \tag{2}$$

with μ representing the magnitude of an effective force corresponding to the active energy input and $\widehat{P}(t - \Delta t_P)$ is a polarization vector that captures the displacement of the droplet's center of mass over a fixed time window Δt_P. In our simulations, we set $\Delta t_P = 1$ Monte Carlo Step (MCS) and test the robustness of this choice in the Supplementary Material (SM). Vector $\vec{P}$ functions as a memory term, fluctuating due to the stochastic nature of the Monte Carlo method. When multiplied by the activity parameter μ in a new force term, this stochastic variable gives rise to persistent Brownian motion.

Vector $\vec{c}$ represents the displacement of a water pixel at the interface, during a trial spin flip, and is obtained during the simulation as follows: If a gas site turns into water this site is considered the final position and a random neighboring water site is chosen to be the initial position. Otherwise, if a water site changes to gas, this site is considered the initial position while a random neighboring water site is the final position. For simplicity, we assumed that self propulsion fluctuates only on the horizontal plane, without vertical components.

The total run of a simulation is at least 2×10^5 MCS from which the last 10% of the total running time are used to measure observables of interest. Each MCS is composed by V_T number of trial spin flips. A spin flip is accepted with probability $\min\{1, \exp(-\beta\Delta H)\}$, where $\beta = 1/T$ and T acts as noise to allow the phase space to be explored. Here we used $T = 13$ that was shown to have an acceptance rate of approximately 20% for the passive system[15]. The simulation is exemplified in Figure 2(b).

2.3 Pillared surface and the initial configurations

We consider a 3D droplet on a pillared surface, with geometric parameters defined in Figure (1)a. The pillar width is fixed at $w = 5\,\mu$m and the height at $h = 10\,\mu$m, while the interpillar spacing a is varied within the range $a \in [5\,\mu\text{m}, 11\mu\text{m}]$. This yields a roughness ratio—defined as the ratio of the true surface area to the apparent projected area—given by $r = 1 + 4hw/(a+w)^2$, which spans the range $r \in [1.78, 3]$.

To account for the influence of initial conditions, the system is initialized in two different wetting states. The first configuration, referred to as D^0, consists of a droplet in the shape of a sphere tangentially touching the surface, as illustrated in Figure (3)-a. The second correspond to fully wetted case, with contact angles $\theta_c = 90^\circ$, referred as W^0, shown in Figure (3)-b. In both cases, the initial droplet volume is set to $V_T \approx V_0 = \frac{4}{3}\pi R_0^3$, with $R_0 = 50\,\mu$m.

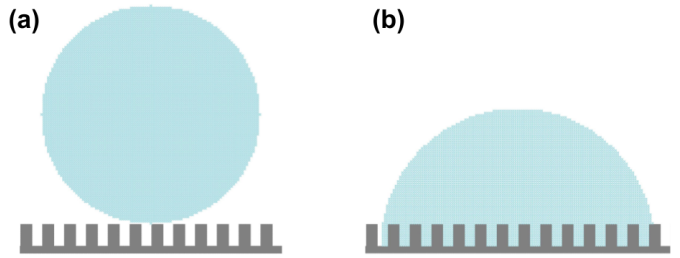

Fig. 3 Two initial wetting configurations used in the Monte Carlo simulations: one in the dry state, refereed as D^0 **(a)** and one in the wet state, W^0 **(b)**.

2.4 Observables

Wetting measures. The apparent contact angle (θ_c) of the droplet is estimated by assuming a spherical shape, which is a valid approximation for the droplet size used here, where interfacial energy dominates over gravitational effects[15,17]. Under this assumption, θ_c is defined as

$$\theta_c = \arcsin\left(\frac{2H.B}{H^2+B^2}\right), \tag{3}$$

where B and H are the base radius and height of the droplet, respectively, measured directly from the simulations. The validity of the spherical approximation is confirmed through circularity measurements and holds for $\mu < 8$, as shown in the SM.

The volume fraction f of liquid penetrating the substrate is calculated as the ratio between the number of liquid pixels located below the pillar height (V_{pu}) and the total volume of the droplet (V), which fluctuates around a target volume V_T during the simulation. In the steady state, this gives $f = \frac{V_{pu}}{V}$.

Dynamical measures. Dynamical proprieties were studied through the calculation of the mean squared displacement (MSD), defined as:

$$|\vec{\Delta}r(\Delta t)|^2 = |\vec{r}(t_0+\Delta t) - \vec{r}(t_0)|^2; \tag{4}$$

where $\vec{r}(t)$ represents the position vector of the center of mass of the droplet at time t. The average is computed over multiple measurements of $|\Delta\vec{r}(\Delta t)|^2$, leading to $MSD = \langle|\Delta\vec{r}(\Delta t)|^2\rangle$.

3 Results and Discussion

3.1 Wetting Measures

Figure (4) summarizes the wetting behavior of the pillared substrates for three different roughness values r. The top row of the figure shows the droplet's most frequent contact angle θ_C for two initial configurations, D^0 and W^0. The middle row displays cross-sections of the droplet for different values of activity μ, while the bottom row presents the fraction of water that penetrates the substrate.

The first column in Figure (4) corresponds to the substrate with the highest roughness ratio explored in this study, $r = 3$. The results show that: i) There is no significant difference in either θ_C or the penetration fraction f, regardless of the initial configuration, indicating that this substrate does not exhibit metastability. ii) Similarly, θ_C and f remain constant across all values of the activity parameter μ. The cross-sectional views visually confirm that the droplet remains in a dry state, regardless of the initial condition or the value of μ. Additionally, for $\mu > 8$, the droplet deviates from a spherical shape, showing visible deformation, which is quantified in the SM.

We emphasize the presence of a horizontal dotted line in Figure (4)a marking the value of the contact angle, θ_C, which is the unique stable state reported in reference[17]. As briefly discussed in the previous section, that study computed the free energy profile for the pillared surface and found that, for this particular roughness value r, there exists a single free energy minimum. This minimum corresponds to a dry state and exhibits the same contact angle θ_C observed in our simulations.

As the roughness ratio r decreases—shown in the second and third columns of Figure (4)—a noticeable difference in both contact angle θ_C and penetration fraction f is observed depending on the initial condition. When the droplet starts from the D^0 configuration, the contact angle remains high ($\theta_C \approx 145^\circ$), and $f \approx 0$ for all values of μ, indicating that the droplet stays in a dry state.

However, when the droplet is initialized in a wetting configuration such as W^0, the behavior changes. Focusing on the middle column, which corresponds to an intermediate roughness value ($r = 2.18$), the contact angle starts at approximately $\theta_C \approx 120^\circ$ for $\mu = 0$, with $f \approx 10\%$. The corresponding cross section confirms that the droplet wets the substrate. As μ increases, θ_C also increases, while the penetration fraction f decreases. At a given value μ_t, the final state becomes identical for both initial conditions. This indicates that above a threshold activity μ_t, the self-propulsion is sufficient to drive the droplet into the dry state, effectively overcoming the energy barrier between metastable states.

For the smallest roughness ratio studied ($r = 1.78$), the droplet always remains in a wet state when initialized in W^0, although it transitions through a series of distinct wetting states characterized by varying values of θ_C and f, as shown in Figure (4)-c,f and can be visually interpreted by the cross sections of the droplets.

We note that these figures also include several horizontal dotted lines, which represent the contact angles of metastable states identified in the reference[17]. This suggests that on substrates with multiple free energy minima, the self-propelled droplet is able to explore a range of metastable states as μ increases. Since the droplet visit more than one wetting minima at a time, some analyses are needed in order to distinguish the most frequent θ_c (see details in the SM).

In the SM, we examine the robustness of the observed metastable states by initializing the droplet in an alternative wetting configuration. The results indicate that the same metastable states are explored as in the case starting from the reference configuration W^0. This suggests that the self-propelled droplet is capable of consistently probing these states. However, some of the metastable states reported in reference[17] are not accessed in our simulations. We attribute this to the shallowness of those free energy minima, which may be easily bypassed due to the relatively high activity of the self-propelled droplet.

Figure (5) shows the relationship between the threshold activity μ_t and the roughness ratio r for various substrate geometries.

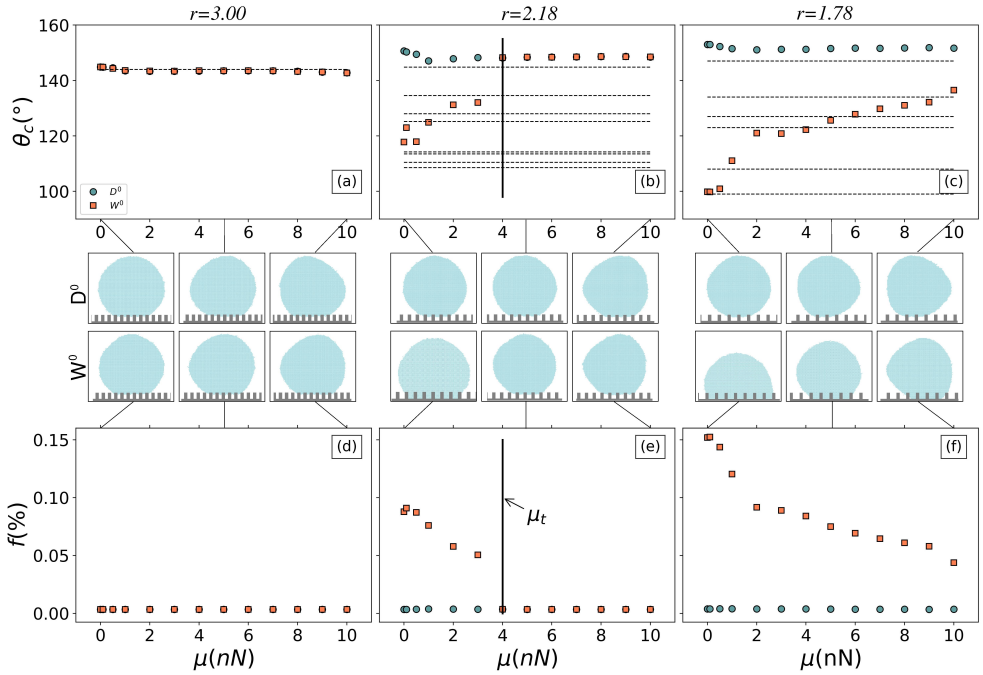

Fig. 4 Wetting properties for three roughness values r. Top row: contact angle θ_C of the droplet as a function of activity μ. Middle row: cross-sections of the droplet for different values of μ. Bottom row: fraction of water penetrating the substrate f as a function of μ. All plots are shown for two initial conditions: D^0 and W^0. The differences in θ_C and f between these initial conditions indicate that substrates with $r = 2.18$ and $r = 1.78$ exhibit metastability, whereas $r = 3$ corresponds to a surface with a single energy minimum. Horizontal dotted lines indicate the values of θ_C associated with the free energy minima reported in Ref. [17].

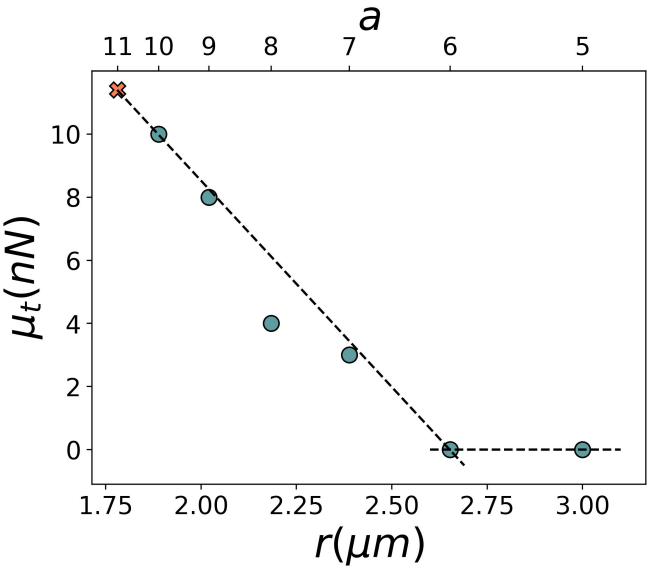

Fig. 5 The threshold value μ_t is shown as a function of the substrate's geometric parameters. The x-axis (bottom) represents the interpillar distance a, while the top axis indicates the corresponding roughness ratio r. When $\mu_t = 0$, the substrate exhibits a single energy minimum. For $\mu_t > 0$, multiple minima emerge, signaling the transition from a non-metastable substrate to one that supports metastable states.

Parameter μ_t serves as an indicator of metastability: $\mu_t = 0$ signifies the absence of metastability in the substrate, while $\mu_t > 0$ indicates the existence of metastable states. Moreover, the results reveal that μ_t decreases approximately linearly as r increases, suggesting that greater self-propulsion is required for the droplet to escape from deeper energy wells associated with lower roughness. This also implies that, for sufficiently high activity, the droplet can overcome energy barriers and effectively suppress metastability, reaching the dry state.

We repeated the measurements of θ_C *vs.* μ for larger values of $\Delta t_P = 10, 100$, and show in the Supplementary Material that the results remain highly robust. This indicates that the self-propelled droplets are effectively probing the substrate's free energy landscape rather than simply undergoing random, activated motion.

3.2 Dynamical Measures

The mean squared displacement (MSD) curves of the self-propelled droplet are shown in Figure 6. Persistent Brownian motion typically exhibits two characteristic regimes: an initial ballistic regime (MSD $\propto \Delta t^2$) followed by a diffusive regime (MSD $\propto \Delta t^1$), though intermediate behaviors may also arise. The transition from ballistic to diffusive motion reveals the persistence length l_P of the self-propelled droplet, representing the typical distance it travels before its polarization direction changes.

For the substrate with roughness ratio $r = 3$ (Figure 6a), no significant differences in droplet dynamics are observed between the two initializations, D^0 and W^0. This supports the notion that this substrate does not exhibit metastability, as discussed in the

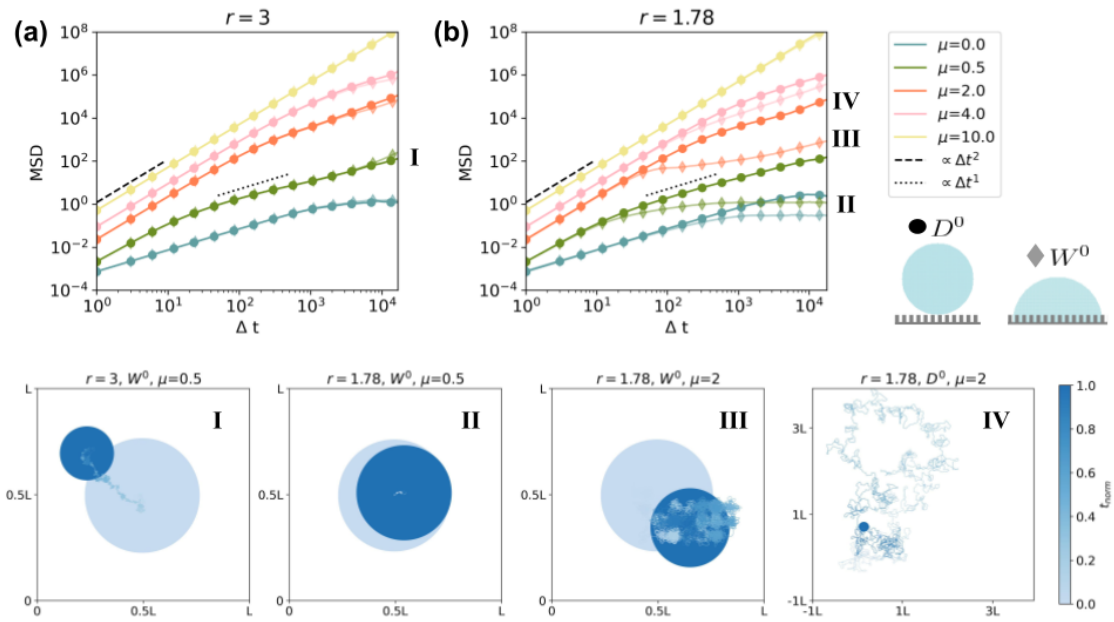

Fig. 6 Dynamical proprieties. Top row: MSD *vs* Δt multiple μ(colors) curves for **(a)** $r = 3$, **(b)** $r = 1.78$. Droplets were initialized in 2 different initial wetting conditions: D^0 (circle marker) and W^0 (diamond marker). Bottom row: Representative trajectories associated with four MSD curves (I, II, III and IV) of droplets starting seat $t = 0$ (ligth blue) until $t = t_{max}$ (dark blue). The circles reproduces the initial and final droplet circumference over the pillars. The parameter sets are: **(I)** $r = 3$, W^0,$\mu = 0.5$; **(II)** $r = 1.78$,W^0,$\mu = 0.5$; **(III)** $r = 1.78$,W^0,$\mu = 2$; (IV) $r = 1.78$,D^0,$\mu = 2$

previous section.

In contrast, for the case $r = 1.78$, shown in Figure 6b, notable behaviors emerge at relatively low values of activity μ. At short times, the ballistic regime appears to be independent of the initial condition. However, beyond this initial phase, the MSD curves diverge, with one trajectory exhibiting higher motility than the other, corresponding to D^0 and W^0, respectively. This effect is particularly evident for $\mu < 4$ in Figure 6b. As μ continues to increase, the curves converge again, suggesting that dynamic observables like MSD are no longer sensitive to the underlying metastability captured by the contact angle θ_C and volume fraction f, as shown in Figure (4).

Across all cases in Figure 6, increasing μ extends the duration of the ballistic regime, consistent with observations in the literature[31,41]. Furthermore, the regime following ballistic motion varies depending on the combination of roughness r, activity μ, and the initial wetting condition. These variations are qualitatively illustrated by representative droplet trajectories in Figures 6I-IV. For $r = 3$—a non-metastable substrate—all values of μ eventually lead the droplets into a diffusive regime, independent of the initial condition. In this scenario, μ primarily determines the scale of both persistent and diffusive motion, as exemplified in Figure 6I.

Conversely, for the metastable substrate with $r = 1.78$, the initial wetting condition plays a critical role. The W^0 initialization can lead to either a trapped state (Figure 6II) or a caged state (Figure 6III), depending on the value of μ. Meanwhile, droplets initialized with D^0 display consistent motile behavior across both substrate types, resulting in a typical diffusive pattern (Figure 6IV).

We tested the robustness of the dynamical behavior with respect to the memory parameter Δt_P (see SM) and found that the MSD is highly sensitive to its value. Larger Δt_P enhances the polarization term, resulting in a delayed transition to the diffusive regime. This sensitivity suggests that MSD alone cannot reliably infer the metastable properties of the substrate. We argue that Δt_P should be chosen such that the persistence length l_P is compatible with the substrate's geometric scale. For instance, if $l_P \gg a$, meaningful information about substrate-induced metastability cannot be extracted from the MSD. Nevertheless, regimes characterized by highly linear droplet motion—where l_P is large—remain physically relevant in other contexts, such as those involving nematic active systems[26,28].

4 Conclusions

In this work, we present a novel approach to investigating wetting metastability by integrating active matter dynamics into a cellular Potts framework[31,41]. Through simulations of self-propelled droplets driven by polarization forces[31,41], we demonstrate how activity modulates access to metastable states on pillared substrates.

We quantified the wetting behavior of the substrate by measuring the droplet's contact angle θ_C and the liquid penetration fraction f, while the mean squared displacement (MSD) was used to assess the droplet's dynamics. The system exhibits configuration-dependent wetting states—a hallmark of metastability. Notably, beyond a critical activity threshold, μ_t, droplets converge to a single dry state, irrespective of initial conditions. This transition implies that self-propulsion energizes droplets sufficiently to surmount inter-state barriers. The threshold μ_t itself emerges as a quantitative descriptor of substrate metastability, scaling linearly with geometric parameters like the roughness ratio, r.

While the wetting observables (θ_c, f) remain robust to variations in the model parameter Δt_P, the MSD shows pronounced sensitivity. This highlights the importance of selecting Δt_P such that the resulting persistence length (l_P) is compatible with the characteristic roughness scales of the substrate, ensuring a physically meaningful interpretation of the dynamics.

Broadly, our work explores the potential of active droplets as adaptive probes for wetting metastability. By mapping local energy minima through measurements of θ_C and f, the approach offers insights that could inform experimental strategies for wettability control and contribute to the design of functional surfaces in applications such as microfluidics and self-cleaning materials[42,43].

Acknowledgements

We thank C. Beatrici for stimulating discussions about this work. We thank the Brazilian agencies Coordenação de Aperfeiçoamento de Pessoal de Nível Superior (CAPES) and the Conselho Nacional de Desenvolvimento Científico e Tecnológico (CNPq) for their support. CB and LB acknowledge funding under grant number CNPq-443517/2023-1. We also thank the supercomputing laboratory VD Lab at IF-UFRGS and the NYU IT High Performance Computing resources, services, and staff expertise, for computer time.

References

1 A. R. Parker and C. R. Lawrence, Nature, 2001, **414**, 33–34.
2 Y.-T. Cheng and D. E. Rodak, Applied physics letters, 2005, **86**, 144101.
3 K. Liu, X. Yao and L. Jiang, Chemical Society Reviews, 2010, **39**, 3240–3255.
4 O. Al-Khayat, J. K. Hong, D. M. Beck, A. I. Minett and C. Neto, ACS Applied Materials & Interfaces, 2017, **9**, 13676–13684.
5 C. Chen, D. Weng, A. Mahmood, S. Chen and J. Wang, ACS applied materials & interfaces, 2019, **11**, 11006–11027.
6 C. Gavazzoni, M. Silvestrini and C. Brito, The Journal of Chemical Physics, 2021, **154**, 104704.
7 R. N. Wenzel, Ind. Eng. Chem., 1936, **28**, 988–994.
8 A. Cassie and S. Baxter, Trans. Faraday Soc., 1944, **40**, 546–551.
9 D. Quéré, Annu. Rev. Mater. Res., 2008, **38**, 71–99.
10 D. Lazzari and C. Brito, Physical Review E, 2019, **99**, 032801.
11 C. Brito, H.-J. Butt and A. Giacomello, The Journal of Chemical Physics, 2023, **159**, 150402.
12 C. Wang and Z. Guo, Nanoscale, 2020, **12**, 22398–22424.
13 M. Sbragaglia, A. Peters, C. Pirat, B. Borkent, R. Lammertink, M. Wessling and D. Lohse, Phys. Rev. Lett., 2007, **99**, 156001.
14 T. Koishi, K. Yasuoka and S. Fujikawa, Proc. Natl. Acad. Sci. U. S. A., 2009, **106**, 8435–8440.
15 H. Fernandes, M. Vainstein and C. Brito, Langmuir, 2015, **31**, 7652–7659.
16 I. Patrícia da Silva Ramos, C. Gavazzoni, D. Lazzari and C. Brito, The Journal of Chemical Physics, 2023, **158**, 154703.
17 M. Silvestrini, A. Tinti, A. Giacomello and C. Brito, Advanced Materials Interfaces, 2021, **8**, 2101005.
18 F. Brochard, langmuir, 1989, **5**, 432–438.
19 X. Yao, H. Bai, J. Ju, D. Zhou, J. Li, H. Zhang, B. Yang and L. Jiang, Soft Matter, 2012, **8**, 5988–5991.
20 M. Lin, P. Kim, S. Arunachalam, R. Hardian, S. Adera, J. Aizenberg, X. Yao and D. Daniel, Physical Review Letters, 2024, **132**, 058203.
21 X. Han, R. Jin, Y. Sun, K. Han, P. Che, X. Wang, P. Guo, S. Tan, X. Sun, H. Dai et al., Advanced Materials, 2024, **36**, 2311729.
22 J.-F. Joanny and S. Ramaswamy, Journal of Fluid Mechanics, 2012, **705**, 46–57.
23 D. Khoromskaia and G. P. Alexander, Physical Review E, 2015, **92**, 062311.
24 A. Doostmohammadi, J. Ignés-Mullol, J. M. Yeomans and F. Sagués, Nature communications, 2018, **9**, 3246.
25 S. Trinschek, F. Stegemerten, K. John and U. Thiele, Physical Review E, 2020, **101**, 062802.
26 F. Stegemerten, K. John and U. Thiele, Soft Matter, 2022, **18**, 5823–5832.
27 L. N. Carenza, G. Gonnella and G. Negro, Out-of-equilibrium Soft Matter, The Royal Society of Chemistry, 2023.
28 R. C. Coelho, H. R. Figueiredo and M. M. Telo da Gama, Physical Review Research, 2023, **5**, 033165.
29 C. Pérez-González, R. Alert, C. Blanch-Mercader, M. Gómez-González, T. Kolodziej, E. Bazellieres, J. Casademunt and X. Trepat, Nature physics, 2019, **15**, 79–88.
30 R. Adkins, I. Kolvin, Z. You, S. Witthaus, M. C. Marchetti and Z. Dogic, Science, 2022, **377**, 768–772.
31 C. Beatrici, C. Kirch, S. Henkes, F. Graner and L. Brunnet, Soft Matter, 2023, **19**, 5583–5601.
32 T. Sanchez, D. T. Chen, S. J. DeCamp, M. Heymann and Z. Dogic, Nature, 2012, **491**, 431–434.
33 G. Ramos, M. L. Cordero and R. Soto, Soft Matter, 2020, **16**, 1359–1365.
34 G. Kokot, H. A. Faizi, G. E. Pradillo, A. Snezhko and P. M. Vlahovska, Communications Physics, 2022, **5**, 91.
35 S. Michelin, Annual Review of Fluid Mechanics, 2023, **55**, 77–101.
36 M. Silvestrini and C. Brito, Langmuir, 2017, **33**, 12535–12545.
37 F. Graner and J. Glazier, Physical review letters, 1992, **69**, 2013.
38 L. de Oliveira, D. Lopes, S. Ramos and J. Mombach, Soft Matter, 2011, **7**, 3763–3765.
39 V. Mortazavi, R. D'Souza and M. Nosonovsky, Phys. Chem. Chem. Phys., 2013, **15**, 2749–2756.
40 C. Stamatopoulos, A. Milionis, N. Ackerl, M. Donati, P. Leudet de la Vallée, P. Rudolf von Rohr and D. Poulikakos, ACS nano, 2020, **14**, 12895–12904.
41 A. J. Kabla, Journal of The Royal Society Interface, 2012, **9**, 3268–3278.
42 R. Malinowski, I. P. Parkin and G. Volpe, Chemical Society Reviews, 2020, **49**, 7879–7892.
43 D. Sun and K. F. Böhringer, Micromachines, 2019, **10**, 101.

Supplementary Material: Probing wetting properties with self-propelled droplets

Bernardo Boatini, Cristina Gavazzoni, Leonardo Gregory Brunnet and Carolina Brito

September 23, 2025

1 The measure of the contact angle θ_C: separation of the peaks

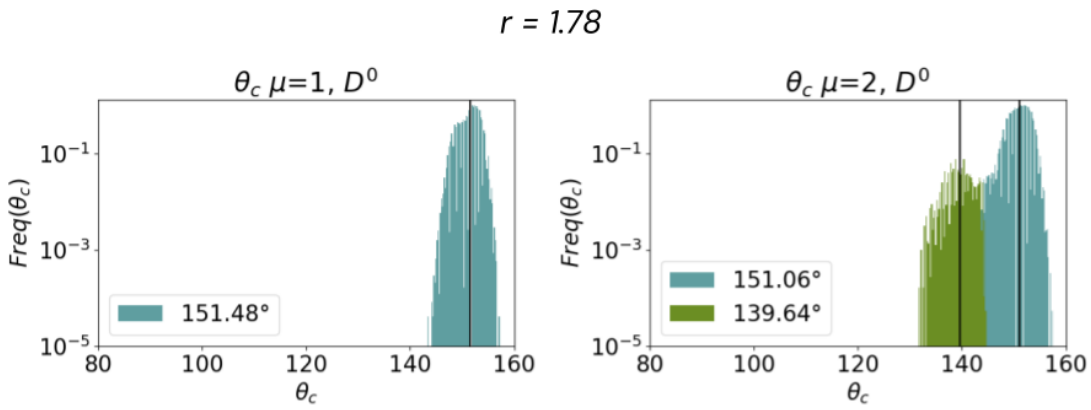

Figure 1: Normalized frequency of two θ_c histograms after the peak separation procedure. For the same roughness ($r = 1.78$) and initialization (D^0): $\mu = 1$ (left) led to a single peak, and $\mu = 2$ (right) led to two peaks . The legend associate the time average value of each cluster to the labeling color.

After confirming that the droplet has reached a steady state by analyzing the curves of θ_C and f as functions of MCS, we select the final 10% of the simulation time and examine the histograms of these quantities. Two typical examples are shown in the Fig. 1, corresponding to different values of μ. Depending on the parameters, multiple peaks may appear in the histogram, indicating ~~that~~ the droplet transitions between distinct θ_C values. Notably, one peak is significantly more dominant than the others—by a factor of 50 to 100—and this trend holds across all parameters studied.

To systematically identify these peaks, we employ the k-means clustering algorithm. This unsupervised method partitions a set of n data points into kk clusters by assigning each point to the cluster with the nearest mean (centroid). Since the number of clusters k is an input of the algorithm, we determine its optimal value using a physically motivated criterion. The procedure for peak identification follows these steps:

1. We test different values of k in the range $k \in [1, 5]$. For each k, we compute the average contact angle $\langle\theta_C\rangle^k$ associated with each cluster;

2. to determine whether k peaks are physically meaningful, we impose a minimum separation threshold $\Delta\theta_C^* = 6°$. Specifically, if $|\langle\theta_C\rangle^k - \langle\theta_C\rangle^{k+1}| < \Delta\theta_C^*$, clusters k and $k+1$ are considered indistinguishable, and thus correspond to the same peak. This threshold is justified by the typical roughness-induced variations in θ_C observed on the substrate.

An example of the clustering result obtained using the above procedure is shown in Fig. 1. The average of θ_C value of the most frequent peak is the one reported in the main text.

2 Droplet shape dependence on μ

To assess the validity of the spherical approximation, a measure of droplet roundness was considered. Given that the water-substrate interface is expected to approximate a circular shape, this approach provides a meaningful evaluation. To quantify this, an ellipsoid regression fit was applied at the droplet pillars contact pixels, and the time series of the minor (r_-) and major (r_+) axes was recorded to compute the normalized circularity (e):

$$e = \frac{r_-}{r_+}.$$

Figure 2 shows the circularity e as a function of activity μ for two different substrates. We find that a spherical shape assumption remains valid for $\mu < 8$, where the average circularity typically satisfies $e \geq 0.9$. Interestingly, even in the passive case, e is not exactly 1, as the droplet may occupy grooves differently along the x and y axes.

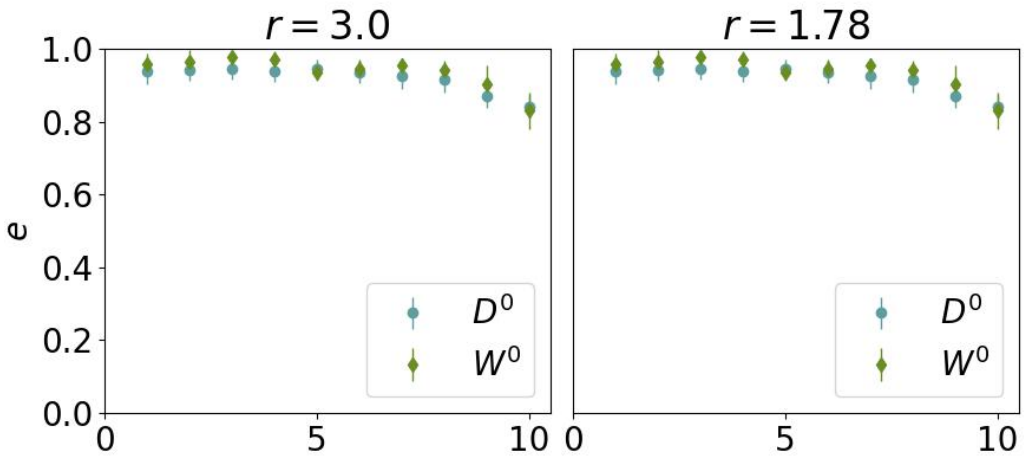

Figure 2: Average circularity e dependence on activity (μ) for distinct initialization: D^0 (blue) and W^0 (green). Each panel represent a different substrates: $r = 3$ (left) and $r = 1.78$ (right).

3 Robustness of the results against Δt_P and the initial conditions

The memory time (Δt_P) parameter is used in the active CPM literature [1, 2]. Despite its apparent consistency, Δt_P is often treated as an adjustable parameter, with its deeper model dependencies left unexplored and unclarified. To investigate this, some relevant values of Δt_P were tested using a reference set of parameters already employed in the main study: $\Delta t_P \in (1, 10, 100)$. The same activity and wetting measurements were conducted for these memory times.

The analysis revealed that Δt_P has a significant impact on the droplet's dynamical behavior, resulting in a rapid increase in persistence as Δt_P increases (Figure 3). This effect is similar to the influence of μ, as both contribute to increasing the persistence length l_P, thereby delaying the onset of the diffusive regime. This finding aligns with previous studies on active nematic droplets, which exhibit both chaotic and linear motion [3, 4, 5, 6].

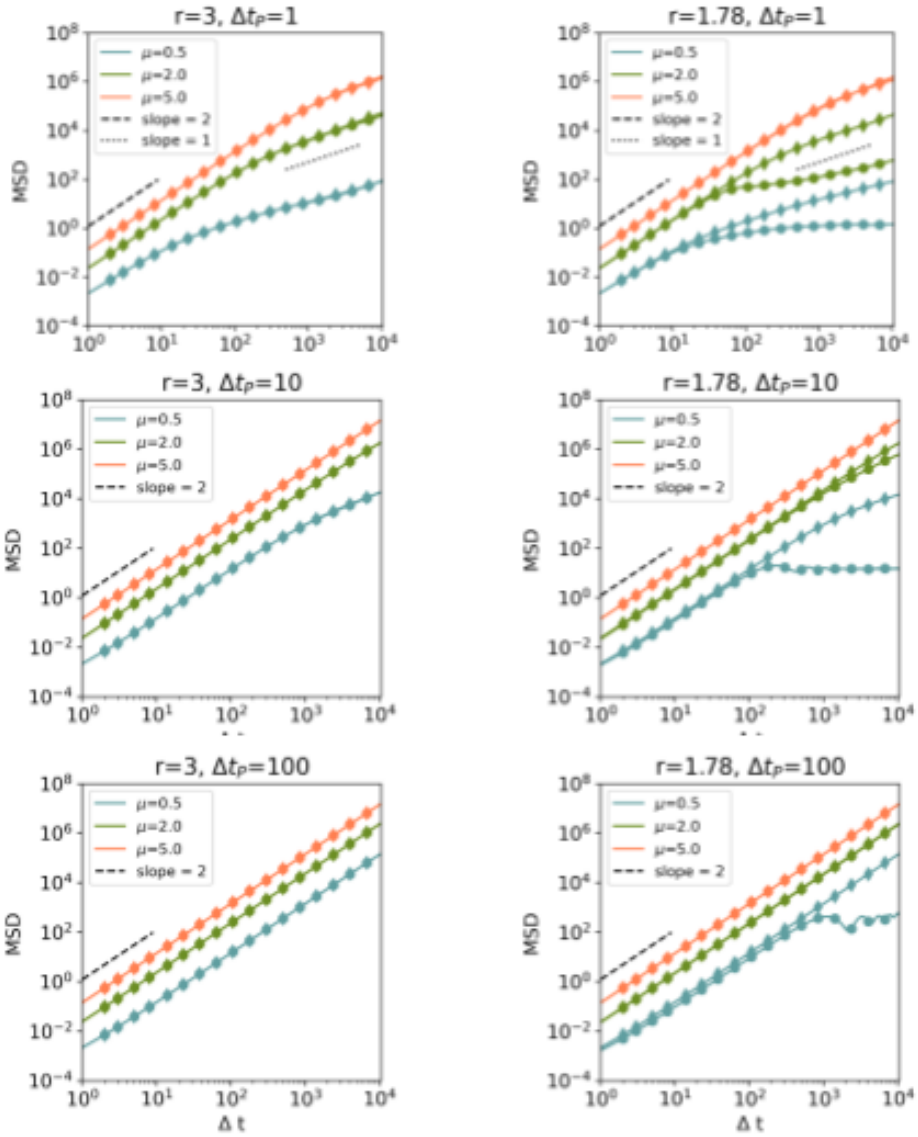

Figure 3: Each MSD frame has a fixed r value and Δt_P with multiple μ (colors) curves. Droplets were initialized in 2 cases: D^0 (diamond marker) and W^0 (circle marker).

Figure (4) shows the influence of Δt_P on the measure of θ_C as a function of the activity μ. We observe that the steady-state wetting quantities remain practically unaffected by Δt_P.

In the main text, we showed how θ_C *vs* μ depends on two initial wetting conditions: a dry state (D^0) and a wet state (W^0). Here, we introduce an additional wet initial condition, referred to as W^1, illustrated in the inset of Fig.5a. This configuration represents an even more extreme wetting case, with an initial contact angle of $\theta_c = 30^0$. Figure5 shows that the droplet visits the same set of states for both W^0 and W^1, indicating the robustness of the results to the degree of initial wetting.

Furthermore, the consistency of the θ_C *vs.* μ curves across larger values of $\Delta t_P = 10, 100$ and different initial conditions suggests that the self-propelled droplets are effectively probing the substrate's free energy landscape, rather than exhibiting purely activated, random motion.

-

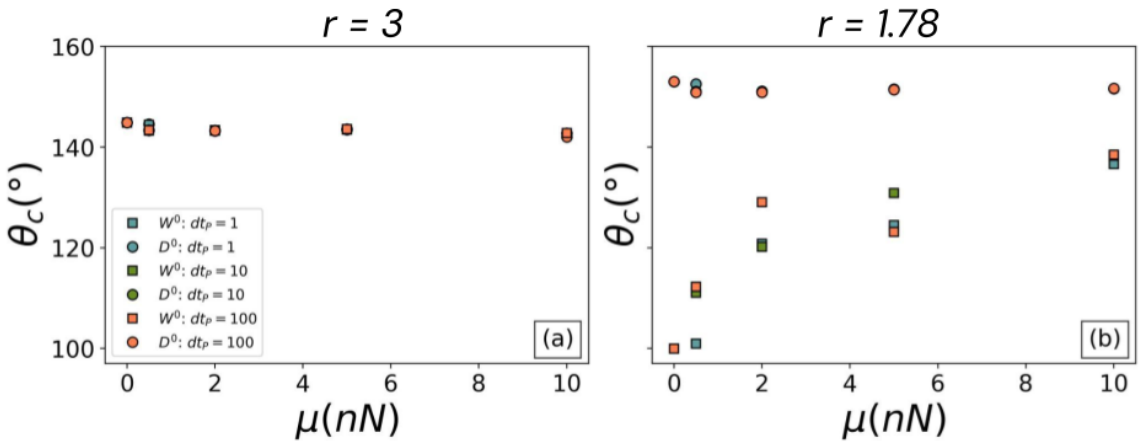

Figure 4: θ_c vs. μ diagrams for fixed $h = 10$ and $r = 3$ (a) or $r = 1.78$ (b) . Each color indicates the the most frequent θ_c for both initial conditions in combination with the explored Δt_P.

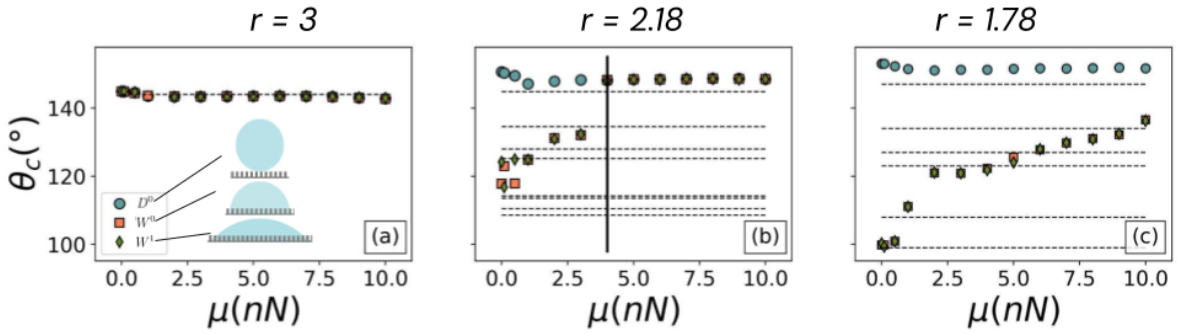

Figure 5: θ_c versus μ diagrams for three substrates. Each point indicates the the most frequent θ_c for three initial conditions: D^0, W^0 (green) and W^1 (red). Horizontal lines in $r \in (3, 2.18, 1.78)$ are the numerical values for each energy minimum found by reference [7].

References

[1] Carine Beatrici, Cássio Kirch, Silke Henkes, François Graner, and Leonardo Brunnet. Comparing individual-based models of collective cell motion in a benchmark flow geometry. Soft Matter, 19:5583–5601, 2023.

[2] Alexandre J Kabla. Collective cell migration: leadership, invasion and segregation. Journal of The Royal Society Interface, 9(77):3268–3278, 2012.

[3] Diana Khoromskaia and Gareth P Alexander. Motility of active fluid drops on surfaces. Physical Review E, 92(6):062311, 2015.

[4] Sarah Trinschek, Fenna Stegemerten, Karin John, and Uwe Thiele. Thin-film modeling of resting and moving active droplets. Physical Review E, 101(6):062802, 2020.

[5] Fenna Stegemerten, Karin John, and Uwe Thiele. Symmetry-breaking, motion and bistability of active drops through polarization-surface coupling. Soft Matter, 18(31):5823–5832, 2022.

[6] L. N. Carenza, G. Gonnella, and G. Negro. Motility and self-propulsion of active droplets. In Out-of-equilibrium Soft Matter. The Royal Society of Chemistry, 03 2023.

[7] M. Silvestrini and C. Brito. Wettability of reentrant surfaces: A global energy approach. Langmuir, 33(43):12535–12545, 2017.